Journal of Micromechanics and Microengineering

Modelling on the droplet formation and optimizing of the microfluidic cartridge used for the microfluidic impact printing

To cite this article before publication: Yuxin Mao *et al* 2019 *J. Micromech. Microeng.* in press https://doi.org/10.1088/1361-6439/ab4cda

IOP Publishing Journal Title
Journal **XX** (XXXX) XXXXXX https://doi.org/XXXX/XXXX

Modelling on the Droplet Formation and Optimizing of the Microfluidic Cartridge Used for the Microfluidic Impact Printing

Yuxin Mao[1,2,#], Xiaojie Wang[1,2,#], Xuan Li[1,2], Baoqing Li [1,2,*], Jiaru Chu[1,2]

[1] *Department of Precision Machinery and Precision Instrumentation, University of Science and Technology of China, Hefei, Anhui, China.*
[2] *Key Laboratory of Precision Scientific Instrumentation of Anhui Higher Education Institutes, University of Science and Technology of China, Hefei, Anhui, China.*
***** *Author to whom correspondence should be addressed. Electronic mail: bqli@ustc.edu.cn*
[#] *Yuxin Mao and Xiaojie Wang contributed equally to this work.*

E-mail: bqli@ustc.edu.cn

Received xxxxxx
Accepted for publication xxxxxx
Published xxxxxx

Abstract

Microfluidic impact printing (MIP), which was proposed recently as a drop-on-demand microdroplet generation technology, shows a promising future in precision liquid handling. However, the working principle of the droplet formation and the performances of the generated droplets from the microfluidic chip are still unclear. In this article, we build a MIP system for multiplexed microdroplet dispensing, and develop a theoretical model to analyze the process of the droplet generation. As a result of the theoretical model which was validated against finite element simulations and experiments, the volume and the ejection velocity of the printed droplets can be predicted, demonstrating that the structure of the microfluidic cartridge plays the core role in the system. Based on the model, we have introduced a converging channel in the design of the cartridge to improve the performance of printing system. Owning to the asymmetric transfer characteristic of the converging channel, the aspirated volume of the air could be reduced by 40% during the membrane restoring, and the liquid in the cartridge reaches stability to the initial pre-printing state faster, that would enable the MIP system to have a wider adjustable range of droplet volume and a higher printing frequency.

Keywords: microfluidic impact printing, flow resistance, converging channel

1. Introduction

Microdroplet has emerged as a promising tool for biochemical applications because of its various advantages, including the miniaturization due to ultra-small volume, the parallelization brought about by large numbers of droplet reactors, and high-efficiency owing to minimal reaction time [1, 2]. In the numerous microdroplet generation approaches (e.g. flow focusing, emulsification and inkjet printing), benefited from the flexibility and convenience of manipulating the droplet size and number, several drop-on-demand (DOD) microdroplet printing methods been demonstrated and were used in the corresponding biochemical applications, such as drug screening, tissue engineering and

immunoassaying [3-5]. And commercial DOD droplet dispensing devices have emerged on the market, which are based on different droplet dispensing principles. For example, MicroFab is based on thermoelectricity, Biojet Elite™ is driven by syringe pump, BioFluidix PipeJet™ and Tecan D300e™ are piezoelectric-based dispensing devices. They all claim to have high quality and low volume droplet dispensing abilities, and among most of these devices, the actuators are integrated with the liquid cartridge expcet for BioFluidix PipeJet™.

Several research groups are working towards the generation of microdroplets and their applications. For example, the Basaran group carried out a computational analysis to simulate the formation of liquid drops of incompressible Newtonian fluids from a simple capillary tube for the purpose of improving the theoretical understanding of drop-on-demand (DOD) ink-jet printing [6]. They also proposed a new method to significantly reduce drop radius by controlling the waveform without reducing nozzle radius [7]. Furthermore, they summarized and discussed the formation of inkjet droplets, and analyzed the application of droplet nonstandard inkjets [8,9]. The Hutchings group studied the application of DOD in the field of inkjet printing, particularly in biomedical areas [10,11].

In many biomedical applications, samples are in small volumes while from various sources [12,13]. If each integrated micro-jet is disposable, the extension and application of these devices would be greatly limited by their high cost. Alternatively, washing is a cheaper choice, but it has the risk of cross-contamination. In order to solve these problems, a series of microdroplet printing devices with interchangeable micro-jet/cartridge and separable actuators have been proposed. The Koltay group reported a device which was named single-cell-manipulator (SCM) with a separable piezo-stack actuator [14]. The Kim group developed a novel nanoliter liquid dispensing system with plug-and-play dispensers and detachable pneumatic pump [15,16]. Furthermore, the Walus group presented a disposable inkjet dispenser technology and demonstrated a Lab-on-a-Printer concept through using an inkjet dispenser and a microfluidic mixer [17]. The non-contact and disposable design of the dispenser shows great potential in reducing cross-contamination and cutting down maintenance costs.

Microfluidic impact printing (MIP), as a novel drop-on-demand microdroplet generation approach with low-cost interchangeable microfluidic cartridge and separable actuator, which enables nano-liter droplets generation in non-contact mode, was firstly introduced by Pan group [18]. Furthermore, a multiplexed, scalable, and compact microfluidic multi-parametric gradient generation system based on the MIP was developed for multi-dimensional studies of synthetic genetic modules in cell-free system [19]. Different from those of previous mentioned nano-liter dispensing technologies [15-17], the refill of liquid in the MIP system is conducted automatically by the combined effect of capillary force in the microchannel and negative pressure generated by the membrane's deformation restoration, which means it doesn't need any additional input from external pump or potential energy. With the design of microfluidic channel and nozzle, the minimum loading volume and dead volume of MIP system are as low as 2μL and 0.25μL, respectively [19].

During the printing process of the MIP, when the flexible membrane of the microfluidic cartridge is deformed by separable actuator, part of the internal fluid is pushed toward the nozzle to form a droplet and the other liquid is pushed back to the inlet simultaneously. When the membrane restores after release of the action, the liquid flows back from both ends (nozzle and inlet) to the deformable chamber under the negative pressure. Meanwhile, following with back-flow of the liquid into the deformable chamber, air may enter the chamber from the nozzle to form bubbles in the microchannel. Due to the compressibility of air, the air bubbles may affect the volume consistency of the dispensed droplets, and even interrupt the next printing. If the air does not enter the chamber and no bubbles are formed in the liquid, the inhaled air in the microchannel could be vented out from the nozzle automatically by capillary force. In summary, the geometry structure of the microfluidic cartridge affects flow distribution under impacting, refill time of the liquid from inlet, and vent time of air out of nozzle, which are all directly related to the printing performances such as droplet volume, ejection velocity, maximum working frequency and stability of printing.

In the previous works [18, 20], many experiments were repeatedly conducted to investigate the effect of cartridge structural parameters on the droplet generation., such as nozzle diameter, membrane deflection and the channel height. Some mathematical equations have been proposed to express a simple relationship between the printed droplet volume and the geometric parameters of the microfluidic cartridge, and some qualitative analysis of the flow resistance design of the cartridge microchannels was carried out. Furthermore, some common shortcomings exist in the DOD printing on small scales, such as droplet evaporation, droplet size variability, printing frequency, liquid adhesion, contamination and channel clogging have been properly addressed or reduced. Increasing printing speed, covering layer of oil and controlling the ambient humidity can reduce evaporation. The droplet size and printing frequency can be controlled by the driving signal. The sizes of maximum and minimum droplet can be adjusted by manipulating nozzle diameter. Superhydrophobic treatment of the nozzle surface using femtosecond laser solves the issue of liquid adhesion [21]. Due to the disposable property, the cartridge can be replaced directly, and the contamination and clogging is no longer a critical issue. However, though pico-liter to nano-liter droplets have been

successfully generated, the lack of completely theoretical models can only allow us to perform some qualitative analysis, which could increase the difficulty of conducting different experiments for multiple case and optimizing cartridge parameters.

In this article, we build a microfluidic impact printing platform through integration of piezoelectric actuator and microfluidic cartridge. We adopted a nozzle-in-plane design of the microfluidic chip for the sake of long-lasting printing and droplet uniformity in direction. A theoretical model and a FEM simulation were established to interpret the mechanism of droplet formation in MIP and discover the influences of the flow resistances distribution on both droplet volume and velocity. Furthermore, a converging structure was introduced in the microfluidic cartridge to achieve asymmetric transfer characteristic of flow during the printing cycle, reducing the volume of aspirated air and stabilization time of fluid, which can improve the robustness and throughput of droplet printing.

2. Experimental Methods

2.1 Microfluidic Impacting Printing (MIP) System

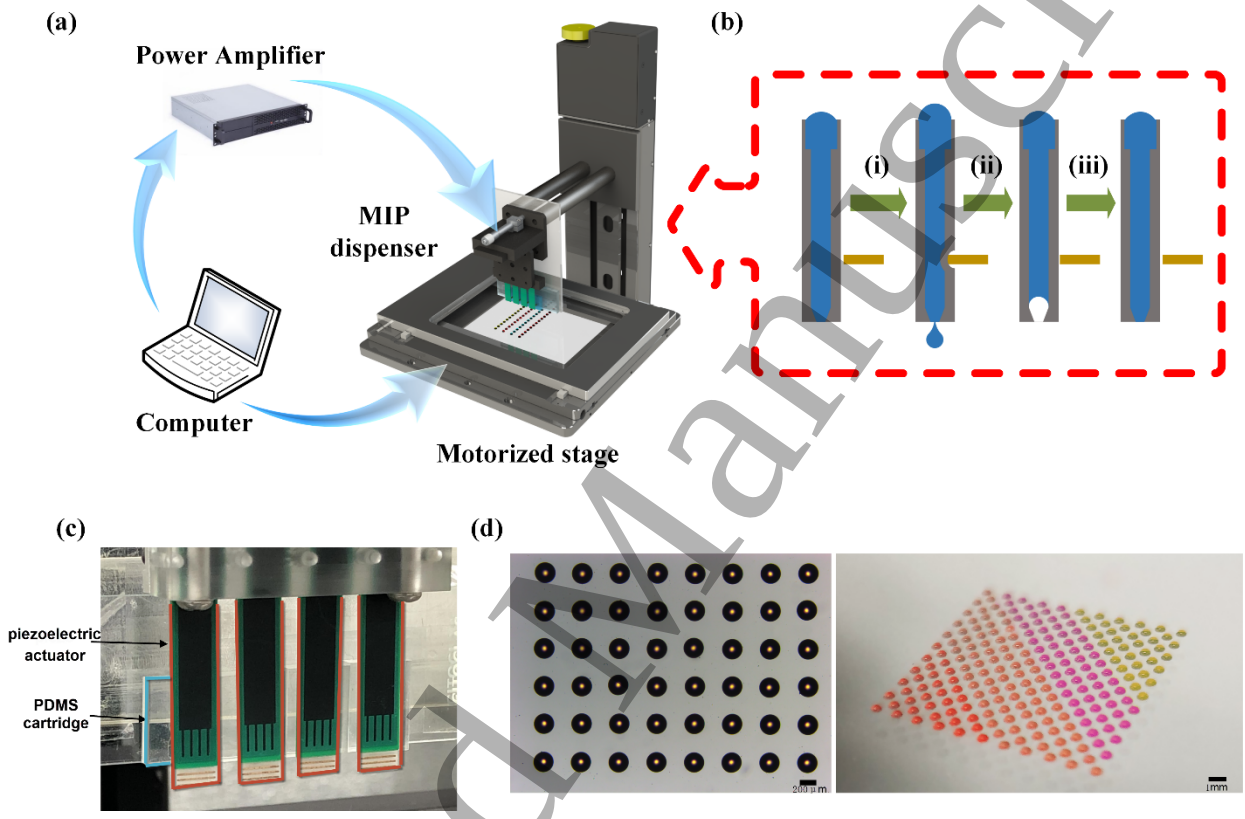

Figure 1. (*a*) Schematic diagram of the 4-channel multiplexed microdroplet dispensation system based on MIP. (*b*) Schematic illustration shows the working principle of microdroplet printing based on MIP, and (*c*) prototype of 4-channels MIP system. (*d*) Microdroplet array generated by the system (scale bar: 200μm,1mm).

A 4-channel MIP system for multiplexed micro-droplet dispensation was built in this study. As shown in Fig.1a, the MIP system comprises a piezoelectric actuator array, microfluidic cartridges, and 3-axis motorized stages (MLS203-2 & LTS150, Thorlabs co.). The piezoelectric actuator array is composed of four piezoelectric bending actuators (PANT Co., QDTE52-7.0-0.82), each of which is fixed at one end and glued with a micro-pin (Keystone Electronics 1374-1) at the other end. Microfluidic cartridge is installed on a clamp vertically, which makes the deformable chamber in align with the pin. Pulses are generated from a computer using D/A card (AC6632, WWLAB co.), then amplified by a home-made voltage amplifier, and lastly applied on the piezoelectric actuator. It's the high-level voltage that makes the actuator generate a strike onto the cartridge, forcing the reagent in the cartridge to eject as droplets from a nozzle (figure 1b (i)). When the applied voltage is in low level, both the actuator and the membrane of the cartridge are retracted to the initial position. The retraction-induced negative pressure could draw liquid to refill the deformed area from both ends, along with air's aspiration from the nozzle (figure 1b (ii)). Be beneficial from the capillary force, liquid is reloaded soon after the retraction, exhausting the air out of the nozzle (figure 1b (iii)). The figure 1c shows the piezoelectric driven 4-channels MIP system.

Utilizing this micro-droplet dispenser, parallel printing of the droplet array can be achieved (figure 1d).

It should be noted that in addition to the control of the driving waveform, the distance between the striker and the microfluidic cartridge can significantly affect the motion state of the actuator. Therefore, a manual stage (DAHENG GCM-1641M) was integrated with the piezoelectric actuators for fine distance adjustment. The diameters of droplets which printed on a PDMS made substrate were measured using a microscope (Leica DMI3000b). Furthermore, a high-speed camera (Photron FASTCAM SA5) was set up to observe the droplets ejection and the movement of fluid in the cartridge during the process of printing.

2.2 The Fabrication of the Microfluidic Cartridge

The microfluidic cartridge consists of two polydimethylsiloxane (PDMS) layers (microchannel layer and deformable membrane layer) (figure 2). A photolithography and a replica molding technique were utilized to fabricate the microchannel layer. Specifically, a microchannel mold with 75μm-thick photoresist (MicroChem SU-8 2025) was patterned on a silica glass wafer by utilizing photolithography (figure 2(i)). An additional acrylic block (2 mm thick, 2 mm width and 10mm length) was glued to the corresponding position of the photoresist to form a mold of reservoir (figure 2(ii)). Next, a mixture of the polydimethylsiloxane prepolymer and curing agent (10:1 w/w, Dow Corning SYLGARD184) which was degassed by vacuum for 15min was poured onto the photoresist mold with 3mm thickness and then cured at 65°C for 2 hours (figure 2(iii-iv)). A 250μm-thick planar PDMS film was prepared as the deformable membrane layer. Then, the two PDMS layers were bonded through oxygen plasma treatment (Mingheng PDC-MG) at 75W and 60Pa for 50s (figure 2(v)). Finally, the dispensing nozzle of cartridge was manually trimmed under a microscope using a scalpel (figure 2(vi)).

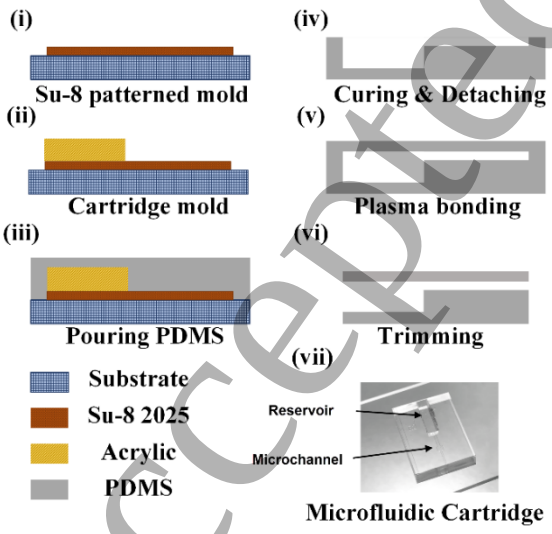

Figure 2. The fabrication process of the microfluidic cartridge.

3. Modelling and Simulation

3.1 Theoretical Modelling

In order to study the fluid dynamics in printing process, a theoretical model based on the fluidic circuit theory [18, 20] was established in this part. The fluid motion in the microfluidic cartridge during the printing process are described through a simplified equivalent fluidic circuit model (figure 3a). The fluid driven by the impact-induced deformation could be assumed as a flow source, of which volumetric flowrate Q_M is dependent on impacting velocity of the actuator [18]. Assume the volumetric flowrate at the inlet and the nozzle are Q_I and Q_N, the flow resistances of each part of cartridge are R_I, R_A, R_B and R_N, respectively. Based on this model, we present several equations that can be used to predict droplet volume, ejection velocity and air aspiration under different experiment conditions. According to the Hagen–Poiseuille equation, the pressure at section A and section B (P_A and P_B) can be expressed as

$$P_A - \frac{4\gamma cos\sigma}{D_I} = (R_A + R_I)Q_I \quad (1)$$

$$P_B - \frac{4\gamma cos\sigma}{D_N} = (R_B + R_N)Q_N \quad (2)$$

where γ is the surface tension of the air–liquid interface and σ is the contact angle between the printing material and the wall of the microchannel, D_I and D_N is the hydraulic equivalent diameter of inlet and nozzle, respectively, which can be calculated by equation (S2). In equation (1) and (2), $4\gamma cos\sigma/D$ denotes the capillary pressure at the nozzle and inlet. The actual diameter of the deformable chamber is 1mm and the depth is only 0.075mm, thus the flow resistance of the deformable chamber ($R_c = 9.09\times10^5$ Pa•s•m^{-3}) is much smaller than those of microchannels ($R_A = 2.08\times10^{11}$ Pa•s•m^{-3}, $R_B = 1.50\times10^{12}$ Pa•s•m^{-3}). To simplify the calculation, we ignored the flow resistance of the chamber during its compression and didn't consider the influence of the fluid viscosity in the chamber. Based on the Bernoulli's principle, the relationship between pressures and volumetric flowrates at section A and B (figure 3a) can be approximately expressed as

$$P_A + \frac{1}{2}\rho\left(\frac{4Q_I}{\pi {D_A}^2}\right)^2 = P_B + \frac{1}{2}\rho\left(\frac{4Q_N}{\pi {D_B}^2}\right)^2 \quad (3)$$

where D_A and D_B is the hydraulic equivalent diameter of microchannel A and microchannel B. In addition, the volumetric flowrates Q_I and Q_N satisfy the equation

$$Q_I + Q_N = Q_M = S\frac{\Delta H}{\Delta t_M} \quad (4)$$

where S is the deformation area of the membrane, ΔH is the impacting-induced deformation and Δt_M is the impacting time. By substituting equation (1), (2) and (4) into equation (3), the relationship between the volumetric flowrate toward the nozzle (Q_N) and the flow resistance (R_A, R_B, R_I, R_N) can be expressed as

$$\frac{4\gamma cos\sigma}{D_I} + (R_A + R_I)(Q_M - Q_N) + \frac{1}{2}\rho\left(\frac{4(Q_M - Q_N)}{\pi {D_A}^2}\right)^2 = \frac{4\gamma cos\sigma}{D_N} + (R_B + R_N)Q_N + \frac{1}{2}\rho\left(\frac{4Q_N}{\pi {D_B}^2}\right)^2 \quad (5)$$

The actual cartridge geometrical specifications are shown in Table 1. In order to facilitate the injection of liquid, the inlet is a square with a side length of 2 mm. According to the equation (S1) and (S2), the flow resistance of inlet R_I is much smaller than others (less than four orders of magnitude), so it can be ignored. Then, the droplet volume (V_N) can be calculated by integrating the volumetric flowrate at the nozzle. Details are shown in Section 4 in the Supplementary Material.

$$V_N = \int_0^{t_M} Q_N \, dt_M = Q_N \bullet \Delta t_M = \frac{8\pi\eta R_A \Delta t_M}{\rho(R_B/L_B - R_A/L_A)}\left\{-\left(\frac{R_B+R_N}{R_A} + 1 + \frac{\rho Q_M}{8\pi\eta L_A}\right) + \left[\left(\frac{R_B+R_N}{R_A} + 1 + \frac{\rho Q_M}{8\pi\eta L_A}\right)^2 + \frac{\rho}{4\pi\eta R_A}\left(\frac{R_B}{L_B} - \frac{R_A}{L_A}\right)\left(Q_M + \frac{\rho {Q_M}^2}{16\pi\eta L_A} - \frac{4\gamma cos\sigma}{R_A D_N}\right)\right]^{\frac{1}{2}}\right\} \quad (6)$$

Table 1. Geometrical specification of the microfluidic cartridge.

Simulation Geometrical Specification			
W_A	*0.4mm*	L_B	*2.6mm*
W_M	*1mm*	L_N	*0.38mm*
W_B	*0.2mm*	D_A	*0.13mm*
W_N	*0.1mm*	D_B	*0.11mm*
L_A	*0.65mm*	H	*0.075mm*
L_M	*1mm*	α	*15°*

Based on this theoretical model, the feature size of droplet printed by MIP system can be predicted in the case of a steady strike of the actuator. Note that the calculation of flow resistance is described in Supplementary Material.

3.2 FEM Simulation Step

For complex geometrical structures that cannot be applied with the theoretical model, a simulation by using finite element method (FEM) was implemented with ANSYS/FLUENT to analyze the dynamic process of droplet printing. The geometry of the cartridge employed in the FEA was shown in the figure 3b, it consists of a nozzle, an impacting deformation chamber, an inlet and microchannels. Considering that the parameters of the cartridge have certain limitations during the fabricating, the parameters of the simulation model were basically determined according to the actual structural parameters. Due to the size of inlet channel which used for loading liquid is much larger than other microchannels, the flow resistance and the surface tension of the liquid at inlet can be ignored. The inlet channel in FEM simulation was simplified as a pressure outlet boundary with liquid phase. The geometrical specifications of cartridge employed in FEM simulation were same as shown in Table 1.

The FEM simulation was carried out by solving the incompressible Navier-Stokes equations. The volume of fluid (VOF) method was used to calculate the two-phase (air phase and fluid phase) flows model during printing. The simulation fluid was dimethyl sulfoxide (DMSO) at 25 °C. The measured contact angle σ between DMSO and PDMS (microchannel wall) is 77°. Uniform pressure outlet boundary conditions were applied at wall of air zone and inlet respectively for the simulation. The pressure–velocity coupling is based on the

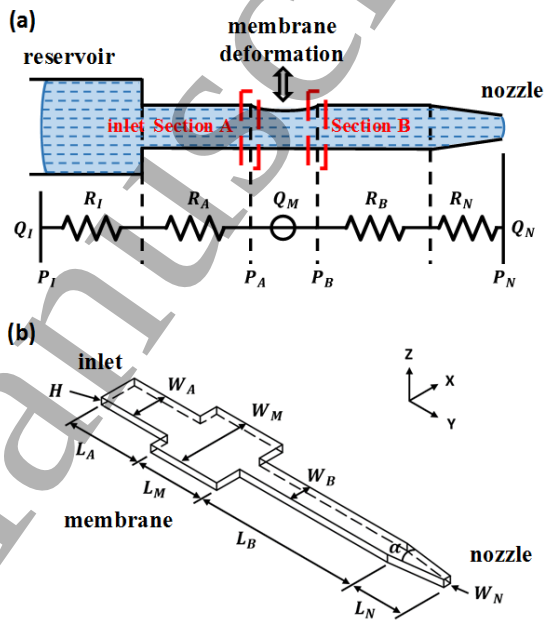

Figure 3. (*a*) The equivalent fluidic circuit model of the MIP. (*b*) Schematic of the geometry of the microfluidic cartridge without reservoir.

SIMPLE algorithm and no-slip boundary conditions were assumed on the microchannel walls. In this model, one side wall of the deformable chamber was set to be movable, and the moving mesh method was used to simulate the impact process of actuator to calculate the fluid dynamics during the droplet printing. The parameters of the moving mesh were shown in Table 2, which were set according to the actually parameters of actuator (the detail measurement steps were presented in Supplementary Material).

Table 2. Parameters of moving mesh.

Moving mesh parameters	
Moving area (diameter)	***0.9mm***
Stroke	***72μm***
Velocity	***0.2m/s***
Dwell time	***2.7ms***

Table 3. Nozzle geometrical specifications of the microfluidic cartridge used in two groups.

Nozzle specifications of microfluidic cartridge							
Nozzle width (W_N)		50μm	75μm	100μm	125μm	150μm	175μm
Nozzle equivalent diameter (D_N)		60μm	75μm	85.7μm	93.75μm	100μm	105μm
Group 1	L_A	882μm	882μm	882μm	882μm	882μm	882μm
	$(R_B+R_N)/R_A$	10	8.9	7.9	7.5	7.2	7.1
Group 2	L_A	882μm	727μm	650μm	610μm	589μm	580μm
	$(R_B+R_N)/R_A$	10	10	10	10	10	10

4. Results and Discussion

4.1 The influence of the flow resistance distribution on droplet volume

In drop-on-demand devices, generating microdroplets with desired volume by adjusting the parameters of the actuator is the most common method. However, in this way, the actuator needs to have high-precision displacement control with high cost [22, 23]. Here, we focus on the structural design of the cartridge to discover the effect of geometric structure on droplet printing. In the following analysis and measurement, the parameters of actuator were set as 80V of driving voltage, 10Hz of operating frequency and 50% of duty cycle. In this case, the average impact velocity of the actuator was 0.2m/s, and the stroke was about 72μm.

Pan group firstly proposed the microfluidic impact printing, and they researched the relationship between the printed droplet volume and the several geometric parameters of the microfluidic cartridge, such as the nozzle diameter and the channel height [18]. In addition, they also supposed that the flow resistance ratio R_n/R_c (the flow resistance from deformable chamber to the nozzle opening and to the inlet opening are R_n and R_c, respectively) may influence the droplet volume, and a qualitative analysis was performed. According to the theoretical model established in equation (5) and (6), the volume of printed droplet depends on the flow resistance of the channel if given a constant volumetric displacement. To research the influence of the the flow resistance distribution on droplet formation, here we conducted a quantitative analyse of its effect. In addition, in order to confirm which of the flow resistance ratio and nozzle size is the dominant factor influencing the droplet volume, we conducted two groups of control experiments for illustration.

In Group 1, only the nozzle size is changed while other structural dimensions were unchanged, which means the flow resistance ratio is varied with nozzle size. As a comparison, L_A is also changed with the nozzle size to maintain a constant flow resistance ratio of 10 in Group 2. In our model of microfluidic cartridge, the flow resistance ratio is the value of $(R_B+R_N)/R_A$, the R_B+R_N is the flow resistance from the deformable chamber to the nozzle, the flow resistance at other toward is R_I+R_A, where $R_I << R_A$, so R_I can be ignored. The detail parameters are shown in Table 3. The FEM simulation was carried out by solving the incompressible Navier-Stokes equation.

Droplet volumes were calculated using both theoretical model and FEM simulations, and verified by experiments, the results of which are summarized in figure 4. In experiment, the droplets are printed on a PDMS substrate, and then calculated using formula [24].

$$V_{droplet} = \frac{(1-cos\sigma)^2(2+cos\sigma)\pi {D_{dot}}^3}{24sin^3\sigma} \quad (7)$$

where the D_{dot} is the diameters of spherical caps which measured by microscope (Leica DMI3000b), the σ is the contact angle between droplet and substrate (the contact angle between DMSO and PDMS is 77°).

The results of the Group 1 were summarized in figure 4 (red solid points), the theoretical calculations (dotted line) and simulation results (circular points) show that the droplet volume is significantly affected by nozzle size, and exhibits a positive correlation. As the nozzle width increases from 60μm to 175μm, the volume of the droplet changes from 6.8nL to 9.5nL. It can be seen from Table 3 that the value of $(R_B+R_N)/R_A$ decreases with increasement of the nozzle equivalent diameter. According to equation (6), the droplet volume has a negative correlation with the value of $(R_B+R_N)/R_A$, which is also demonstrated by the experiment (square points). Due to uncertain factors such as manual error, environmental influence and measurement error, the measured droplet volume range is 6.4nL~10nL. As expected, the trendency of the droplet volumes in Group 2 (blue hollow points in figure 4) is completely different when the value of $(R_B+R_N)/R_A$ is kept constant. The droplet volumes vary over a small range (6.8nL~7.6nL in theoretical and simulation results, 6.4nL~7.3nL in experiment results). Especially when the nozzle equivalent diameter is greater than 90μm, the droplet volume is close to constant, the change of which is within 0.1nL. It can be seen from the results of the two groups, the change in nozzle size does not significantly affect the droplet volume while maintaining the value of $(R_B+R_N)/R_A$. This is

because the when $(R_B+R_N)/R_A$ is constant, the (1/D) term becomes weaker at higher values of D. A verifcation is presented in figure S3 in the Supplementary Material. This illustrated that channel flow resistance is the key factor in the geometric parameters of the microfluidic cartridge that affect droplet volume.

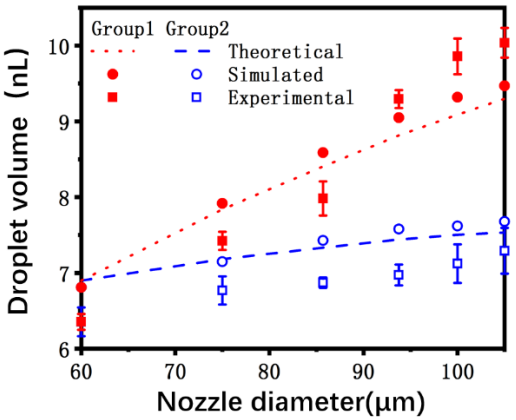

Figure 4. Relationship between nozzle's equivalent diameter and droplet volume in Group 1 and Group 2.

Table 4. The flow resistance ratios with different rear channel lengths.

$(R_B+R_N)/R_A$	L_A (mm)
2	*3.23*
6	*1.08*
10	*0.65*
14	*0.46*
18	*0.36*

Since the flow resistance distribution of the microchannels has a more significant influence on the droplet volume in the MIP system, we subsequently investigated the droplet characteristics at different flow resistance ratios by only changing the channel length L_A. Detail parameters are provided in Table 4. Meanwhile, the channel geometric parameters associated with R_N and R_B were set to constants (the details are in Table 1).

As shown from figure 5a, both the theoretical prediction by equation (6) and the simulation result using FEM reveal the droplet volume decreases as the ratio of (R_B+R_N) to R_A increases. When the ratio is changed from 2 to 18, the theoretical volume is reduced from 13.5nL to 6.3nL, and the simulated volume is reduced from 14.5nL to 7.1nL. The controlled experimental result has same trend which decreases from 12.9nL to 6.5nL. The consistent results show that even the nozzle size is fixed, droplet volume can be regulated by changing the flow resistance ratio (the value of $(R_B+R_N)/R_A$), demonstrating that the flow resistance distribution plays a more importance role in the droplet generation process. The green dotted points in figure 5a represent the coefficient of variation (CV = 100 (S.D./Mean)) of the droplet volume in the experimental measurements. When the $(R_B+R_N)/R_A$=2, the droplet has largest volume (12.9nL), and the satellite droplets formed due to Rayleigh instability cause the CV of the droplet volume to exceed 6%. When $(R_B+R_N)/R_A$ ranges from 4 to 18, no significant satellite droplets appeared, the CV of the printed monodisperse droplets volume were within 3%. The minimum CV of the droplet volume was 2.2% when $(R_B+R_N)/R_A$=10. Then, as the flow resistance ratio increases, the CV of the droplet volume increases because the lower ejection velocity of droplet (figure 5b) makes it easier to adhere to the nozzle, reducing the uniformity of the droplet.

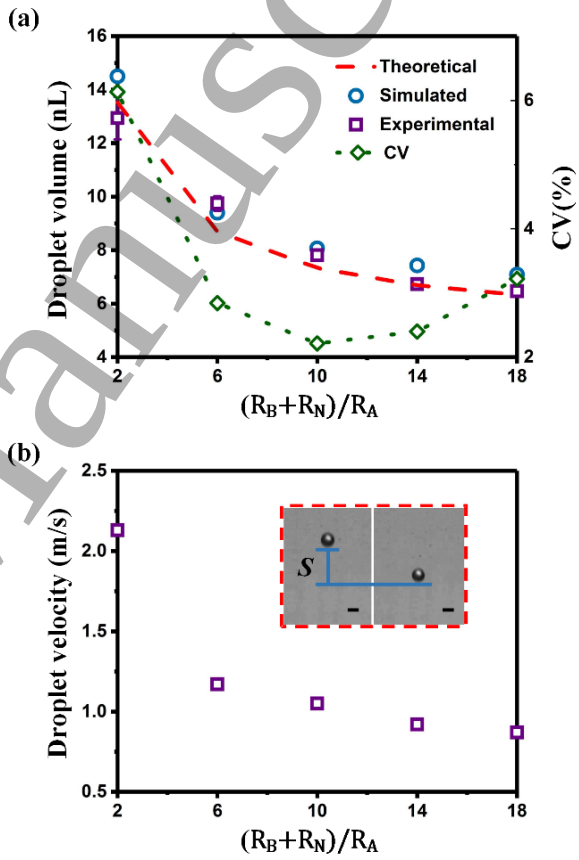

Figure 5. The volumes (*a*) and velocities (*b*) of the droplets printed by MIP system at difference value of $(R_B+R_N)/R_A$. The insert graph is the printed droplet captured by high-speed camera (scale bar: 200μm).

The ejection velocity of droplet, which is estimated according to the droplet's falling distance and time from a high-speed camera, was measured to evaluate the influence of the flow resistance ratio. The velocity measurement procedure is described in Supplementary Material. As shown in figure

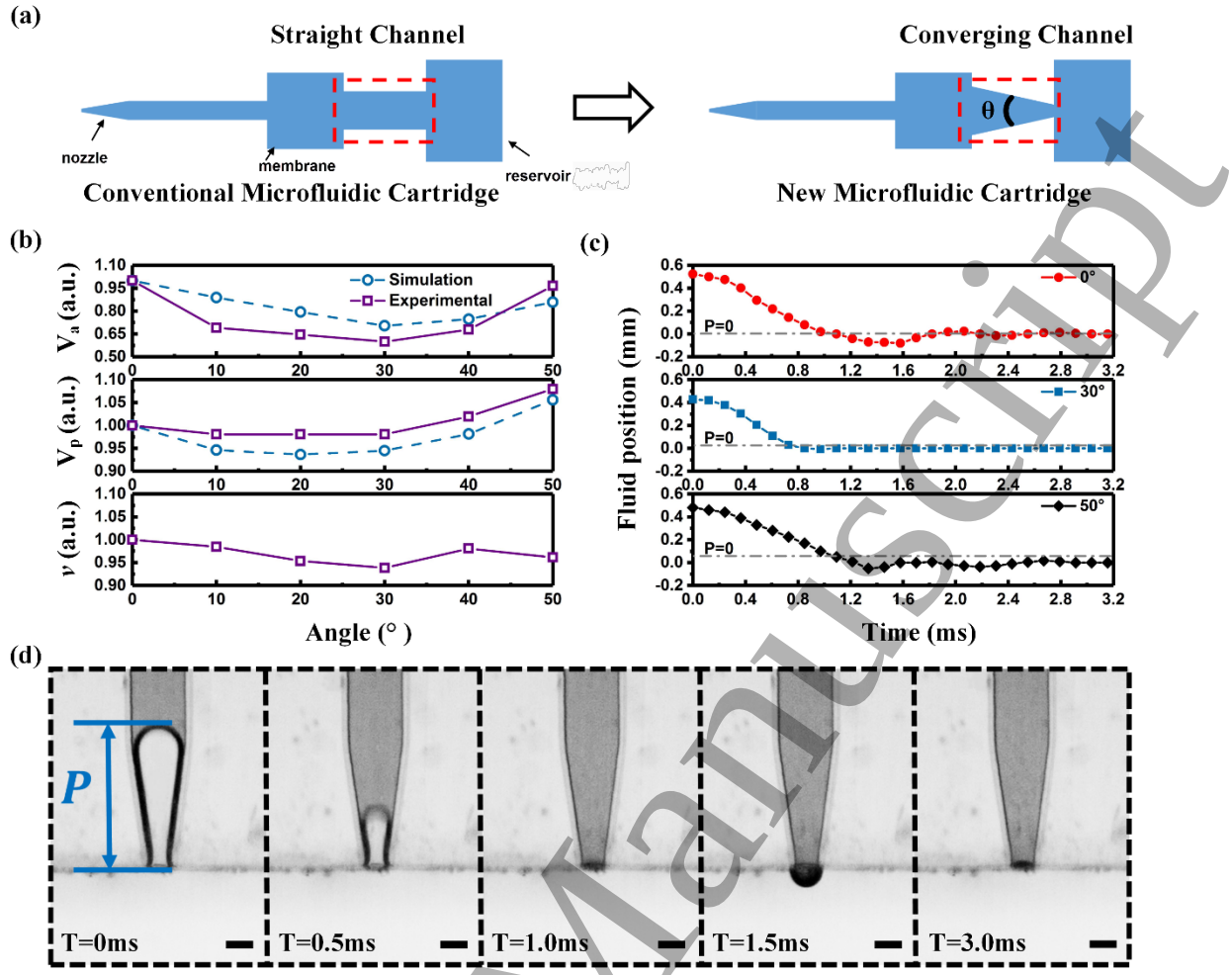

Figure 6. (*a*) Schematic of the conventional microfluidic cartridge and optimized microfluidic cartridge integrated with converging microchannel. (*b*) The performances of the droplet printing at different convergence angles, where V_a is the aspirated volume of the air, V_p is the printed volume of droplet and the v is the ejection velocity of droplet. (*c*) The relationship between P and the time, the dashed line of $P = 0$ represents the position of the liquid at the nozzle. The settling times of three cartridges approximately are 2.8ms, 1.0ms and 2.8ms, respectively. (*d*) High-speed images of the initialization phase (conventional cartridge), P is the distance of the liquid from the nozzle (scale bar: 100μm).

5b, the droplet ejection velocity decreases from 2.1m/s to 0.9m/s, when the value of $(R_B+R_N)/R_A$ increases. It means larger ratio (i.e. smaller inlet resistance) makes less displaced fluid in the chamber flow toward nozzle, as well as the liquid has smaller kinetic energy.

In summary, the volume of droplet generated by microfluidic impact printing can be predicted by the proposed theorectical theory. This theory discovers the relationship between the droplet volume and the structural parameters. As shown by equation (6) and verified by using both simulation and experiments, it's the flow resistance distribution that contributes most to the volume and velocity of the droplet, not the nozzle's flow resistance as normal thought. Moreover, the theory could also be used to model the air aspiration process after retraction, since it's just a symmetric solution of equation (5).

4.2 Optimizing the structure of cartridge

As has been illustrated in figure 1b, the total cycle of droplet printing in MIP includes three phases: droplet printing phase (Phase I), membrane restoration phase (Phase II) and fluid re-loading phase (Phase III). In addition to the first printing phase discussed in section 4.1, the other two phases also affect the printing performances, such as printing frequency and printing stability. At Phase II, fluids flow towards the deformable chamber from the inlet and the nozzle. Meanwhile, air is also aspirated into the microchannel through the nozzle. At Phase III, fluids refill the entire microchannel with air exhausted from the nozzle due to capillary force. The excessive aspirated air during membrane restoring would not only induce longer fluid refilling and stabilization time, which is directly related to the waiting time between successive

printing actions, but also cause air bubbles mixing with fluids in the cartridge, which could stop the following printing. In order to improve the printing stability and printing frequency, it's necessary to minimize the volume of the aspirated air. The volume of aspirated air can be calculated by taking the restoration time (Δt_R) instead of the impacting time (Δt_M) in equation (6). It can be deduced that, like the trendency of the droplet volume, the aspirated air volume is also negatively correlated with the value of $(R_B+R_N)/R_A$. However, reducing the volume of aspirated air by increasing the flow resistance ratio of $(R_B+R_N)/R_A$ would also induces the reductions of droplet's volume and velocity. Therefore, it has become a challenge in the MIP system to aspirate air less on the premise of keeping sufficient droplet velocity.

Here, we introduced a converging microchannel instead of the equal cross-section channel in the design of the microfluidic cartridge, which is derived from the design of the valve-less micropump (figure 6a) [25-29]. Unlike the equal cross-section channel, the converging microchannel offers a lower flow resistance in one direction, and larger flow resistance in the opposite direction [25, 26], which means the R_A at Phase II will be less than that at Phase I. Due to this asymmetric transfer characteristic of the converging channel, the volume of aspirated air can be reduced while keeping the droplet volume and ejection velocity stabilizing.

A series of microchannels with difference convergence angles (θ is from 0° to 50°) were explored in the cartridge. All microchannels have equal hydraulic equivalent diameter in converging direction, which were calculated according to the conclusion proposed by Agrawal group that the equivalent cross section locates at L/3.6 from the narrower end [26, 29]. Utilizing the FEM simulations and experiments, the convergence angle θ was optimized to minimize the aspiration volume of air. The results are summarized in figure 6b, showing the performances of the droplet printing (droplet volume, ejection velocity, volume of aspirated air and stabilization time) at different angles. The first graph in figure 6b shows the relationship between the volume of the aspirated air (Va) and the convergence angle of the microchannel. Both experimental and simulation results show the volume of aspirated air reaches its minimum at θ = 30°, which is nearly 40% less than that of the straight microchannel. While in the droplet printing phase, as shown in second and third graphs in figure 6b, the relative variations of the printed droplet volumes (Vp) and ejection velocities (v) are within 8%, which can be considered to be substantially constant at different convergence angles.

In order to ensure better consistency of the printed droplets, the liquid in the cartridge needs to have a same initial state when printing starts. Therefore, the printing of the next droplet should be started after the fluid refilling and stabilization to the initial state. In brief, the fluid stabilization time can directly affect the frequency of droplet printing. Utilizing a high-speed camera, the stabilization process was illustrated in figure 6d. During this phase, the fluid first fills the microchannel under the driving of the capillary force, but at this time the kinetic energy of the fluid causes a part of it flow out from the nozzle and then retracts into the microchannel due to the surface tension. After several oscillations, the fluid will stabilize at the initial position. In the stabilization phase, the distance of the fluid (P) from the nozzle is used to characterize the process of the fluid stabilizing. The image analysis of this process has been conducted on three different cartridges (of 0°, 30°and 50° angle, respectively), and the results are summarized in figure 6c, where the process of fluid stabilizing at different convergence angles are clearly illustrated. We consider the fluid is stable in the initial state when the amplitude of the P is less than 10μm. The stabilization time of the cartridge with angle of 30° is only 1.0ms, while the time of the cartridge with angle of 50° is 2.8ms.

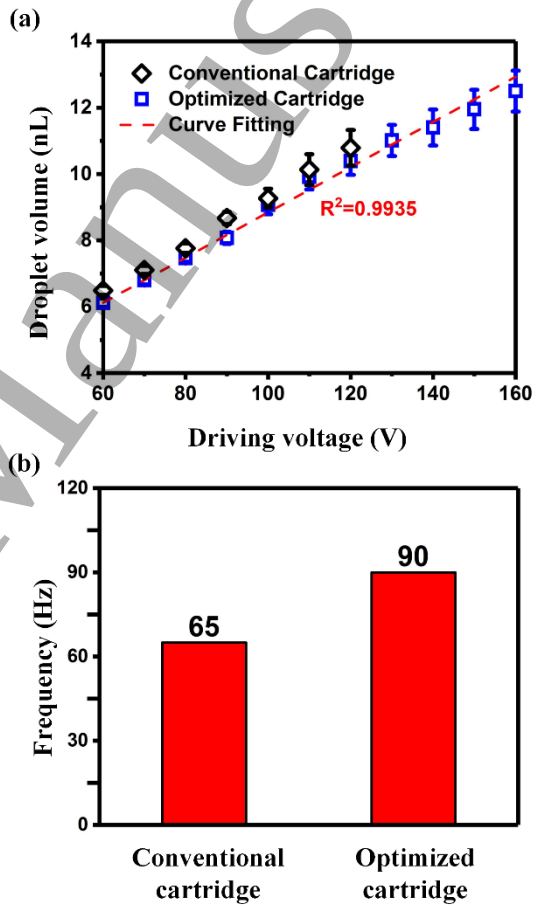

Figure 7. (*a*) The relationship between driving voltage and droplet volume. (*b*) Maximum droplet printing frequency when using two types of microfluidic cartridges.

In the microfluidic impact printing system, droplet volume can be controlled by regulating the driving voltage of the actuator. However, this volume has a certain range because when the voltage is too low, liquid cannot be ejected from the nozzle. If the voltage is too high, more air could be aspirated into the cartridge to form bubbles which affects the

corresponding droplet printing. For the optimized microfluidic cartridges, the volume of aspirated air is reduced at the same driving voltage. Figure 7a compares the relationship between driving voltage and droplet volume when using an optimized microfluidic cartridge and a conventional microfluidic cartridge. The ranges of driving voltage of conventional cartridge and optimized cartridge (convergence angle is 30°) are 60~120V and 60~160V, respectively. As a result, the volume of droplet produced by conventional cartridge ranges from 6.5 to 10.8 nL, while by the optimized cartridge, it is ranging from 6.1 to 12.5nL. Additionally, the shorter stabilization time brought by the optimized cartridge enables a higher frequency of droplet printing. Figure 7b shows the maximum working frequency of stable droplet printing when using the two cartridges, 65Hz for conventional cartridge and 90Hz for the optimized cartridge with 30° converging microchannel.

In summary, compared with the traditional cartridge, the optimized cartridge has a larger voltage range and frequency range, and less air aspiration. The stability and droplet volume range of the MIP system can be significantly improved.

5. Conclusions

In this article, a theoretical model was established to study the mechanism of droplet formation during the microfluidic impact printing. Through theoretical calculation and FEM simulation, a relationship between the flow resistance of the microchannel of the cartridge and the droplet volume has been proposed. Verified by experiments, the volume of the droplet decreases from 12.9nL to 6.5nL as the $(R_B+R_N)/R_A$ increases from 2 to 18. The similar trendency of the droplet ejection velocity was decrease from 2.1m/s to 0.9m/s. In order to reduce the volume of air which aspirated into the cartridge during printing, a converging microchannel has been integrated into the cartridge. Utilize the asymmetric transfer characteristic of the converging microchannel, the volume of air aspirated can be reduced, simultaneously ensure that the fluid has suitable droplet volume and ejection velocity. By optimizing the angle of the converging microchannel, the volume of the aspirated air is reduced by 40%, and the time required for re-loading and stabilizing is reduced from 2.8ms to 1.0ms, which both expand the volume range of the printed droplets to 6.1~12.5nL, and improves the droplets generation rate from 65Hz to 90Hz. In summary, the simulation model proposed in this paper enables the prediction and evaluation of the performance of the printing droplet by using MIP under complex conditions, and also benefits to analysis and optimization of the microfluidic cartridge structure, thereby facilitating the MIP employed in various potential applications.

Acknowledgements

This work is supported by the National Natural Science Foundation of China (Grant No. 51675505), and the Joint Research Fund for Overseas Chinese, Hong Kong and Macao Young Scientists of the National Natural Science Foundation of China (Grant No. 51929501). The authors would like to acknowledge the USTC center for Micro-and Nanoscale Research and Fabrication for technical support in microfabrication.

References

[1] Huebner A, Sharma S, Srisa-Art M, Hollfelder F, Edel J B and Demello A J 2008 *Lab Chip* 8 1244-54

[2] Kaminski T S and Garstecki P 2017 *Chem. Soc. Rev.* 46 6210-26

[3] Gudapati H, Dey M and Ozbolat I 2016 *Biomaterials* 102 20-42

[4] Ng W L, Lee J M, Yeong W Y and Win Naing M 2017 *Biomater. Sci.* 5 632-47

[5] Russell H. Colea, Shi-Yang Tang, Christian A. Siltanen, Payam Shahia, Jesse Q. Zhang, Sean Poust, Zev J. Gartnera and Abate a A R 2017 *Proc. Natl. Acad. Sci. U.S.A* 114 8728-33

[6] Xu, Q. and Basaran, O.A., 2007. Computational analysis of drop-on-demand drop formation. *Physics of Fluids*, 19(10), p.102111.

[7] Chen, A.U. and Basaran, O.A., 2002. A new method for significantly reducing drop radius without reducing nozzle radius in drop-on-demand drop production. *Physics of fluids*, 14(1), pp.L1-L4.

[8] Basaran, O.A., 2002. Small - scale free surface flows with breakup: Drop formation and emerging applications. *AIChE Journal*, 48(9), pp.1842-1848.

[9] Basaran, O.A., Gao, H. and Bhat, P.P., 2013. Nonstandard inkjets. *Annual Review of Fluid Mechanics*, 45, pp.85-113.

[10] Castrejón-Pita, J.R., Martin, G.D., Hoath, S.D. and Hutchings, I.M., 2008. A simple large-scale droplet generator for studies of inkjet printing. *Review of Scientific Instruments*, 79(7), p.075108.

[11] Castrejon-Pita, J.R., Baxter, W.R.S., Morgan, J., Temple, S., Martin, G.D. and Hutchings, I.M., 2013. Future, opportunities and challenges of inkjet technologies. *Atomization and sprays*, 23(6).

[12] Ding Y, Li J, Xiao W, Xiao K, Lee J, Bhardwaj U, Zhu Z, Digiglio P, Yang G, Lam K S and Pan T 2015 *Anal. Chem.* 87 10166-71

[13] Du G S, Pan J Z, Zhao S P, Zhu Y, den Toonder J M and Fang Q 2013 Cell-based drug combination screening with a microfluidic droplet array system. *Anal. Chem*. 85 6740-7

[14] Streule W, Lindemann T, Birkle G, Zengerle R and Koltay P 2004 *JALA* 9 300-6

[15] Choi I H, Kim H, Lee S, Baek S and Kim J 2015 *Biomicrofluidics* 9 064102

[16] Kim H, Choi I H, Lee S, Won D J, Oh Y S, Kwon D, Sung H J, Jeon S and Kim J 2017 *Sci. Rep.* 7 46260

[17] Bsoul A, Pan S, Cretu E, Stoeber B and K. W 2016 *Lab Chip* 14 3351-61

[18] Ding Y, Huang E, Lam K S and Pan T 2013 *Lab Chip* 13 1902-10
[19] Fan J, Villarreal F, Weyers B, Ding Y, Tseng K H, Li J, Li B, Tan C and Pan T 2017 *Lab Chip* 17 2198-207
[20] Li B, Fan J, Li J, Chu J and Pan T 2015 *Biomicrofluidics* 9 054101
[21] Mao Y, Pan Y, Li X, Li B, Chu J and Pan T 2018 *Lab Chip* 18 2720-9
[22] Gan H Y, Shan X, Eriksson T, Lok B K and Lam Y C 2009 *J. Micromech. Microeng.* 19 055010
[23] Zhao L, Yan K C, Yao R, Lin F and Sun W 2016 *J. Manuf. Sci. Eng.* 139 011005
[24] Qian L, Lan H and Zhang G 2018 *Appl. Phys. Lett.* 112 203505
[25] Chandrasekaran A and Packirisamy M 2011 *J. Micromech. Microeng.* 21 045035
[26] Duryodhan V S, Singh S G and Agrawal A 2014 *J. Micromech. Microeng.* 24 125002
[27] Stemme E and Stemme G 1993 *Sens. Actuat. A Phys.* 39 159-67
[28] Wang J, Aw K C, McDaid A and Sharma R N 2015 *Heat Mass Transfer* 52 913-23
[29] Duryodhan V S, Singh S G and Agrawal A 2013b Liquid flow through a diverging microchannel. *Microfluid. Nanofluidics* 14 53–6